

Mass-loss rates for hot luminous stars: the influence of line branching

S. A. Sim^{*}

Astrophysics Group, Imperial College London, Blackett Laboratory, Prince Consort Road, London, SW7 2BW, UK

17 November 2018

ABSTRACT

The effect of photon frequency redistribution by line branching on mass-loss rates for hot luminous stars is investigated. Monte Carlo simulations are carried out for a range of OB-star models which show that previous mass-loss calculations which neglect non-resonance line scattering overestimate mass-loss rates for luminous O stars by ~ 20 per cent. For luminous B stars the effect is somewhat larger, typically ~ 50 per cent. A Wolf-Rayet star model is used to investigate line branching in the strong wind limit. In this case the effect of line branching is much greater, giving mass-loss rates that are smaller by a factor ~ 3 from computations which neglect branching.

Key words: radiative transfer – methods: numerical – stars: mass-loss – stars: individual: ζ Pup – stars: Wolf-Rayet

1 INTRODUCTION

It has been known for over thirty years that luminous, hot stars have powerful stellar winds (Morton 1967). These winds are important in a variety of astrophysical contexts, most notably because of their dynamical influence on the interstellar medium, their effect on stellar evolution and their role in metal enrichment of galaxies.

The proposal that these winds are driven by radiation pressure, in particular by photon scattering in spectral lines, was developed by Lucy & Solomon (1970) and is now generally accepted (Kudritzki & Puls 2000). Since the identification of the mass-loss mechanism, attention has been concentrated on the development of techniques which can predict reliable mass-loss rates. Currently, the most accurate mass-loss rates for hot stars are obtained from Monte Carlo simulations of radiation transport in winds (de Koter, Heap & Hubeny 1997; Vink, de Koter & Lamers 1999, 2000; hereafter VdKL99, VdKL00 respectively), an approach to mass-loss calculations first applied by Abbott & Lucy (1985, hereafter AL85). In this method, the global constraint of energy conservation is used to determine the mass-loss rate algebraically while the wind terminal velocity is fixed at the observed value. This is in contrast to other techniques, such as ‘CAK’ theory (Castor, Abbott & Klein 1975), where the mass-loss rate is an eigenvalue determined at a critical point and the terminal velocity is calculated. Monte Carlo simulations have also been used to study mass-loss as a function of metallicity (Vink, de Koter & Lamers 2001) and mass-loss from luminous blue variables (Vink & de Koter 2002).

A weakness of previous determinations of mass-loss rates from Monte Carlo simulations is the assumption that all line scattering events may be treated as resonance scatterings. This assumption was made by AL85 and has been followed by others in subsequent work (including the mass-loss calculations of de Koter et al. 1997 and VdKL99,00). It has the advantage of significantly simplifying the computation and can be justified for many of the strong lines, even some non-resonance lines, in several important ions (see AL85). However, although remarkably successful for computing mass-loss rates, the assumption is not valid in general: Lucy (1999b) included downwards branching in a Monte Carlo spectral synthesis code for supernovae and found this to have a significant impact on the emergent spectrum.

Following recent developments of the Monte Carlo energy-packet technique (Lucy 2002, 2003), it has become feasible to lift the resonance scattering assumption and allow branching to occur in line scattering events. Branching may effect mass-loss rates since it allows photon leakage from one part of the spectrum to another (see e.g. the discussion by Owocki & Gayley 1999). If only resonance scattering is permitted, the frequency of a given photon packet is gradually redshifted in the frame co-moving with the stellar wind (which accelerates outwards in the star’s reference frame): photons have no opportunity to jump in frequency. Branching alters this by allowing photons to be re-emitted in a different part of the spectrum following a line scattering event. The net effect of line branching on many photons is to preferentially redistribute photons from regions of the spectrum with many strong spectral lines (e.g. ultraviolet) to relatively sparse regions (e.g. infrared). This will reduce

^{*} s.sim@imperial.ac.uk

the net line force since photons undergo fewer line scatterings. The purpose of this paper is to quantify this effect and determine the extent by which the assumption of resonance scattering causes mass-loss rates to be overestimated. It is to be expected that the magnitude of the effect will depend on the typical number of scatterings that photons undergo as they traverse the wind: in the limit where no photons are scattered more than once (single scattering limit) the frequency of re-emission is irrelevant to the mass-loss calculation meaning that line branching can have no effect.

Most of the results presented in this paper relate to OB stars, the stars for which VdKL00 have computed mass-loss rates. However, calculations appropriate for Wolf-Rayet (W-R) stars are also presented. The winds of W-R stars present the greatest challenges to the theory of radiation driven mass-loss, requiring significantly higher efficiency in the transfer of momentum from the radiation field to the matter than OB star winds. Lucy & Abbott (1993, hereafter LA93) investigated line driving in W-R stars and concluded that it was possible to obtain wind performance numbers $\eta \equiv \Phi v_\infty c / L_*$ which are significantly in excess of one, as required for W-R winds (Φ is the mass-loss rate, v_∞ is the terminal velocity of the wind and L_* is the luminosity of the wind-free star). de Koter et al. (1997) performed Monte Carlo simulations with relatively sophisticated models for specific WN5h and Of/WN stars (as classified by Crowther & Dessart 1998) to compute line-driven mass-loss rates for comparison with values determined from H α observations. They found that the computed mass-loss rates were too small by factors $< \sim 2$ (note, however, that there are significant uncertainties in the mass-loss rates determined from observations). A complete understanding of the mass-loss mechanism in W-R stars does not yet exist, but it seems certain that line and continuum driving have some role (see e.g. Nugis & Lamers 2002; Lamers & Nugis 2002). This investigation is of particular relevance to W-R stars because the high density and ionisation stratification of W-R winds means that multiple scattering is much more prevalent than in OB stars. Since the effect of line branching on the radiative acceleration can only be important when multiple scattering occurs, W-R stars should exhibit the most extreme effects.

Subsequent to the commencement of the work presented here, Onifer & Gayley (2003) have published a complementary study of frequency redistribution in stellar winds. They present a parameterised analytical theory appropriate for an idealised spectrum consisting of two frequency domains, one line-rich and the other line-poor. However, they did not perform any calculations with a real line list meaning they were unable to obtain quantitative estimates of the effect of frequency redistribution on mass-loss rates. In contrast, the numerical computations that are presented here do not require any idealisations of the distribution of line opacity across the spectrum and use a real line list, allowing quantitative results to be derived.

Study of line branching is also relevant for predictions of ionising fluxes from hot stars. Calculations which neglect line branching, for example *CoStar* models (Leitherer et al. 1996, Schaerer & de Koter 1997), may overestimate the ionising flux as a result (Crowther et al. 1999). The new Monte Carlo techniques employed here (Lucy 2002, 2003) will readily allow this effect to be quantified in the near future.

In Section 2, the stellar wind models that will be used for the mass-loss calculations are discussed. The Monte Carlo approach used for computing mass-loss rates is described in Section 3, and Section 4 introduces the atomic data used in the calculations. The results for models of OB stars are presented in Section 5 and for a W-R star model in Section 6. Conclusions are drawn in Section 7.

2 MODELS

2.1 Velocity and density

As discussed above the objective of this paper is a *differential* study of the effects of line branching and not the development of high quality stellar wind models. Therefore, simple “core-halo” models are adopted for the sake of tractability. They have been constructed following AL85 and LA93.

The one-dimensional velocity law

$$v(r) = v_c + (v_\infty - v_c) \left(1 - \frac{R_c}{r}\right)^\beta \quad (1)$$

is adopted where R_c is the core radius (the base of the wind) and v_c is the wind velocity at R_c . The adopted values of R_c , v_c , v_∞ and β are given in Sections 5 and 6. The mass density ρ is determined from the equation of mass conservation

$$4\pi r^2 \rho v = \Phi \quad (2)$$

2.2 Ionisation and excitation

The approach to ionisation and excitation recommended by Lucy (2003) is adopted here. Namely, only approximate non-LTE solutions are pursued and analytic formulae are used for both ionisation and excitation. This approach has been used in many previous studies (including AL85 and, in part, VdKL99,00) and is particularly suitable for this study since it decouples the Monte Carlo simulation of the radiation field from the computation of level populations. This provides two advantages: first the need for iteration when constructing models is removed and, more importantly, it allows direct study of the effect of line branching on the radiation field in isolation, without any feedback influence on the level populations.

For ionisation, the modified nebular approximation is adopted

$$\frac{N_{j+1} N_e}{N_j} = [\zeta_j W + (1 - \zeta_j) W^2] \sqrt{\frac{T_e}{T_R}} \left(\frac{N_{j+1} N_e}{N_j}\right)_{T_R}^* \quad (3)$$

where N_j is the number density of the j th ionisation stage, N_e is the free electron number density, W is the dilution factor which is defined in terms of the photospheric radius (R_p) following LA93, ζ_j is the fraction of recombinations to ion j that go direct to the ground state, T_e is the electron temperature and T_R is the radiation temperature. The last bracket in equation (3) is the ionisation fraction computed using the Saha equation at temperature T_R . The partition functions used for this calculation are non-LTE, having been computed using diluted Boltzmann population ratios for non-metastable levels (see below). The ζ -values used

by AL85 have been adopted throughout this paper. The radiation and electron temperatures used for the calculations are discussed in Sections 5 and 6.

When determining level populations, following AL85 and VdKL99, a distinction is made between metastable levels and those with permitted electric dipole decay routes. For a metastable level i , the population relative to the ground state 1 is assumed to be given by the Boltzmann formula

$$\frac{n_i}{n_1} = \left(\frac{n_i}{n_1} \right)_{T_R}^* \quad (4)$$

while for all other levels it is assumed that the population is driven by radiation such that

$$\frac{n_i}{n_1} = W \left(\frac{n_i}{n_1} \right)_{T_R}^* . \quad (5)$$

Equations (3), (4) and (5) allow all level populations to be determined for a given value of ρ . Although approximate, Springmann & Puls (1998) have demonstrated that in a typical O star, these formulae provide excellent approximations to ion/level populations obtained from much more detailed non-LTE calculations.

3 THE RADIATION FIELD

The radiation field is simulated by a Monte Carlo calculation using the Macro Atom approach developed by Lucy (2002). The principles of the method are discussed by Lucy (2002,2003). The details of the Monte Carlo simulation used here are presented below, with particular emphasis on the differences between the calculations discussed by Lucy and those performed here.

3.1 Discretization of model

For the Monte Carlo calculation, the wind models (Section 2) are discretized into a series of thin spherical shells. The velocity is allowed to vary in accordance with equation (1) throughout the model, but all other parameters are taken to be constant within each shell. To evaluate the density (ρ), for each shell equation (2) is used for twenty different values of r which are equally spaced in $x = R_c/r$ between the inner and outer boundaries of the shell. The adopted density for the shell is the x^{-4} -weighted mean of these twenty values. (This weighting is chosen to preserve mass in spherical geometry.) The dilution factor (W) is evaluated at the mid-point of each shell. The innermost shell lies on the surface of the core $r = R_c$, the outermost shell extends to $r = 100R_c$. Typically 100 shells of equal thickness in $x = R_c/r$ are used in the calculations.

3.2 Creation of r -packets

The Monte Carlo quanta used in the simulation are indivisible packets of radiative energy, termed r -packets by Lucy (2002). The Monte Carlo method imposes radiative equilibrium by conserving both the number of packets and their co-moving energy throughout the calculation. Thus packets

are not created in the domain of the simulation but are only launched into the inner shell (from the surface of the star) and propagate until they either re-enter the star through the lower boundary of the innermost shell or emerge from the upper boundary of the outermost shell.

The radiation field incident from the stellar core is modelled by a black-body spectrum at the temperature of the stellar surface $T_e(R_c)$. A lower limit to the wavelength of the incident spectrum is imposed at $\lambda_{\min} = 228 \text{ \AA}$ on the assumption that higher energy photons are immediately removed via bound-free absorption by He II.

The frequencies ν of the incident r -packets are equally spaced in $\ln \nu$, and their energies are assigned according to the Planck spectrum. Packets are created with wavelengths up to $100\lambda_{\min}$. The initial direction cosines μ are chosen randomly, assuming no limb-darkening. Typically, 2×10^6 packets are used in the calculation.

3.3 Propagation of packets

As the packets propagate through the wind they undergo interactions with the material in the wind. Immediately after their creation at the lower boundary, after a packet crosses a shell boundary and also after any interaction with wind material, the optical depth that a packet will traverse before its next interaction is chosen at random using $\tau = -\ln z$ where z is a random number in the interval 0 to 1. Contributions to the optical depth along the packet's flight path from both continuous and line opacity are then considered to determine whether the packet undergoes a continuum scattering, a line absorption or whether the packet will cross a boundary into another shell. The method for selecting which event occurs follows closely that described by Lucy (2003), sec. 5, and the reader is referred to that paper for a full explanation. The subsections that follow briefly explain how the continuum and line contributions to the opacity are computed.

3.3.1 Electron scattering

The only continuum process included in the calculations is scattering by free electrons. Although bound-free processes are important in spectral synthesis, they are not the dominant contribution to the radiation driving force in OB stars and are therefore not important in this differential study of line branching.

Electron scattering is assumed to be isotropic and coherent in the co-moving frame.

3.3.2 Line absorption

The large velocity gradients in a stellar wind mean that line processes can be treated in the Sobolev limit. Lucy (2002) gives expressions for the Sobolev radiative rates and optical depth for the case of an atmosphere in homologous expansion (his equations 20, 21 and 22). However, for the case of non-homologous expansion in a stellar wind, these expressions must be generalised. The radiative rates for spontaneous emission and absorption in the transition between upper level i and lower level j are given by the standard expressions

$$R_{ij} = A_{ij}\beta_{ij}n_i \quad \text{and} \quad R_{ji} = (B_{ji}n_j - B_{ij}n_i)\bar{J}_{ji} \quad (6)$$

where A and B are the usual Einstein coefficients, the n 's are level populations (number densities) and \bar{J}_{ji} is the integrated mean intensity in the line. The escape probability, β_{ji} is given by (Klein & Castor 1978)

$$\beta_{ji} = \frac{1}{2} \int_{-1}^1 \frac{1 - e^{-\tau_s(\mu)}}{\tau_s(\mu)} d\mu \quad (7)$$

and the Sobolev optical depth $\tau_s(\mu)$ is

$$\tau_s = -(B_{ji}n_j - B_{ij}n_i) \frac{h\nu_{ij}}{4\pi} \frac{1}{d\nu/ds} \quad (8)$$

where ν_{ij} is the line frequency and

$$\frac{d\nu}{ds} = -\frac{\nu_R}{c} \left[(1 - \mu^2) \frac{v}{r} + \mu^2 \frac{dv}{dr} \right] \quad (9)$$

is the rate of change of co-moving frequency with path-length for a photon with rest frame frequency ν_R at radius r travelling in the direction specified by μ . The dependence of τ_s on $d\nu/ds$ does not significantly complicate the Monte Carlo calculation since $d\nu/ds$ may be taken as constant along any given photon trajectory within a shell, provided that the shells are sufficiently thin.

In this formulation, the interaction between a packet and a spectral line with which it comes into resonance is described by a single scattering event. In reality, when a photon enters resonance with a line it may scatter many times in that line before it is redshifted out of the region in which interaction occurs (the *resonance zone*). Since thermalisation is not included here, these multiple interactions with a particular line are readily described by a single scattering event and the usual Sobolev escape probability (see de Koter et al. 1997 for a discussion of thermalisation during multiple interactions within a resonance zone). Accordingly, throughout this paper the term *single scattering* is used to refer to photon packets that interact with *one line* during the Monte Carlo simulation, even though this interaction may physically consist of several scatterings. *Multiple scattering* refers to energy packets that undergo two or more independent interactions with *different* spectral lines during their flight through the model.

The Sobolev optical depth of a line is used to determine whether or not a packet is absorbed when it comes into resonance with the line. If absorption occurs the Macro Atom method developed by Lucy (2002) is used to determine the atomic level from which re-emission occurs and a random number is used to determine in which of the transitions from the level the packet is emitted, following Lucy (2003). The Macro Atom formalism does allow for collisional, bound-free and free-free processes but, for simplicity, these are not included here.

The calculation of the Macro Atom upward jumping probabilities requires \bar{J} to be known for each spectral line. Lucy (1999b,2003) has shown how efficient Monte Carlo estimators may be constructed for integrals of the radiation field. Following Lucy, the estimator used here for a transi-

tion between upper level i and lower level j in a particular shell p is

$$\bar{J}_{ji} = -\frac{1}{4\pi\Delta t} \frac{1}{V_p} \sum \frac{1}{d\nu/ds} \frac{1}{\tau_s} (1 - e^{-\tau_s}) \epsilon \quad (10)$$

where Δt is the time interval represented by the Monte Carlo simulation and V_p is the volume of the shell p . The sum runs over all packets which come into resonance with the line in shell p during the simulation. ϵ is the packet energy in the co-moving frame and τ_s is the Sobolev optical depth of the transition. Note that since τ_s is angle dependent every packet encounters a different optical depth: thus the factors involving τ_s must be placed inside the summation. For the branching calculations presented in the later sections of this paper, the \bar{J}_{ji} -values are calculated iteratively for each model, with initial values taken as a dilute black-body radiation field. The values of \bar{J}_{ji} were found to converge to sufficient accuracy for the mass-loss calculations within only one or two iterations.

For all the models discussed in this paper, in addition to finding mass-loss rates when branching is permitted, calculations have been performed in which the Macro Atom formalism has not been employed, and all lines have been treated as resonance lines (no line branching). The comparison of results using the full Macro Atom approach and the resonance scattering assumption forms the basis of the differential analyses presented in Sections 5 and 6.

Once the emission frequency of the packet is determined, the new direction of propagation is determined by randomly sampling the distribution function for the escape probability. Thus the probability of emission with direction cosine μ is

$$P(\mu) d\mu = K \frac{1 - e^{-\tau_s(\mu)}}{\tau_s(\mu)} d\mu \quad (11)$$

where K is a normalisation constant.

3.4 The mass-loss rate

Once all the packets have propagated through the model and have either escaped from the upper boundary or re-entered the stellar core, the rate of energy deposition in the wind can be computed. It is given by AL85

$$L_T = L_* \frac{\sum_k \epsilon_k - \sum_j \epsilon_j - \sum_i \epsilon_i}{\sum_k \epsilon_k - \sum_j \epsilon_j} \quad (12)$$

where the ϵ 's are the rest frame packet energies and the sums run over all packets as they enter the calculation (index k), escape the wind (index i) and re-enter the star (index j). This energy goes into lifting material out of the gravitational field of the star and so the mass-loss rate implied by the Monte Carlo calculation is given by (LA93)

$$\Phi_{MC} = \frac{2L_T}{v_\infty^2 - v_c^2 + v_{esc}^2} \quad (13)$$

where v_{esc} is the escape speed at $r = R_c$. This can be compared to the mass-loss rate assumed in the modelling (Φ). By performing calculations for models with different values

Table 1. The elements and ions included in the line list.

Element	Ions	Element	Ions
H	I	He	I,II
C	I – IV	N	I – VI
O	I – VI	F	I – VI
Ne	I – VI	Na	I – VI
Mg	I – VI	Al	I – VI
Si	I – VI	P	I – VI
S	I – VI	Cl	I – V
Ar	I – V	K	I – V
Ca	I – VI	Ti	I – VI
Cr	I – VI	Mn	I – VI
Fe	I – VI	Co	I – VI
Ni	I – VI		

of Φ , $\Lambda = \Phi_{\text{MC}}/\Phi$ can be found as a function of Φ and so the self-consistent value of Φ (i.e. when $\Lambda = 1$) can be identified.

This approach does not look for local dynamical consistency between the driving force and the velocity law: the mass-loss rate is determined algebraically from the global requirement $\Lambda = 1$ rather than as an eigenvalue at a critical point in the flow. LA93 used this method and showed that, for their W-R model, the Monte Carlo radiative line acceleration differed locally from that implied by the assumed velocity law by up to 0.29 dex. Ultimately models with realistic calculations of the line acceleration which impose local dynamic consistency are desirable but, as discussed by LA93, in view of the other simplifications made, to pursue local consistency here is not warranted.

4 ATOMIC DATA

Atomic models and radiative transition probabilities are needed for the computation of the mass-loss as described above. For the calculations presented here, the atomic data has all been taken from the Kurucz & Bell (1995) atomic database. All elements with solar abundances $X/H < 3 \times 10^{-8}$ have been neglected. For the elements which are included all ionisation stages up to VI that are in the database are used (higher ionisation species are not important for the OB-star models below). The elements and ionisation stages from which lines have been included in the calculations presented in Section 5 are listed in Table 1.

For each ion a cut-off in $\log gf$ was made to exclude weak transitions (in order that the line list is of a manageable size). Atomic models were then constructed for each ion, based on its line list and a complete, frequency ordered line list assembled for the computations. In total, around 2.5×10^5 transitions are included in the line list.

5 OB STARS

In this section, calculations of mass-loss rates for O and B stars will be presented. The models used here have all been constructed using a velocity law (equation 1) with $\beta = 1$, $v_c = 0$ and the density determined from equation (2). In all cases the core radius (R_c) is determined from the luminosity (L) and effective temperature (T_{eff}) using the Stefan-

Table 2. Stellar parameters used for ζ Puppis. From Puls et al. (1996).

Parameter	Value
Mass, M_*	52.5 M_{\odot}
Luminosity, L_*	$10^6 L_{\odot}$
Effective temperature, T_{eff}	42,000 K
Terminal velocity, v_{∞}	2250 km s $^{-1}$

Boltzmann equation. The electron temperature, T_e is assumed to be constant throughout each model and is set by

$$T_e = 0.9T_{\text{eff}} . \quad (14)$$

For their model of ζ Puppis, AL85 adopted a constant radiation temperature somewhat lower than the effective temperature of the star. A similar approach is used here. In principle the radiation temperature for each ion may be determined iteratively during the Monte Carlo simulation (see e.g. Lucy 1999a). Iterative calculations of T_R were performed using the ζ Pup model discussed below in which the radiation temperature for each ion was computed using the simulated radiation field above its ground state ionisation edge. The results of these calculations could be adequately described by a constant value of T_R for ionisation edges below that of He II and no radiation above this edge owing to the truncation of the incident radiation field at 228 Å. Therefore, to avoid the need for iteration, in the OB star calculations that follow

$$T_R = T_{\text{eff}} - 9,000 \text{ K} \quad (15)$$

is adopted for ions with ionisation potentials less than He II and no ionisation to higher ions is included. The decrement of 9,000 K is larger than the decrement adopted by AL85 and was chosen in order to give reasonable agreement between the models presented here and the more sophisticated models used by VdKL00.

5.1 ζ Pup

The first model that will be used to show the differential effect of line branching on mass-loss calculations is chosen to represent the well studied O4 I (f) star, ζ Puppis. The adopted stellar parameters are taken from Puls et al. (1996) and listed in Table 2. There is significant uncertainty in the mass: the Puls et al. value was derived spectroscopically rather than from evolutionary calculations (evolutionary masses are typically higher – e.g. 70 M_{\odot} as adopted by Lamers & Nugis 2003). The same element composition used by AL85 is assumed: i.e. enhanced helium, but all other abundances assumed to be solar.

To investigate the effect of line branching on the mass-loss rate of ζ Puppis a range of models with different input values of Φ have been used to compute $\Lambda(\Phi)$ (see Section 3.4), initially including the complete treatment of line branching. Separate calculations were then performed to find $\Lambda(\Phi)$ when line branching is neglected and all line scatterings are treated as resonant scattering. Fig. 1 shows $\Lambda(\Phi)$ versus Φ for both sets of calculations.

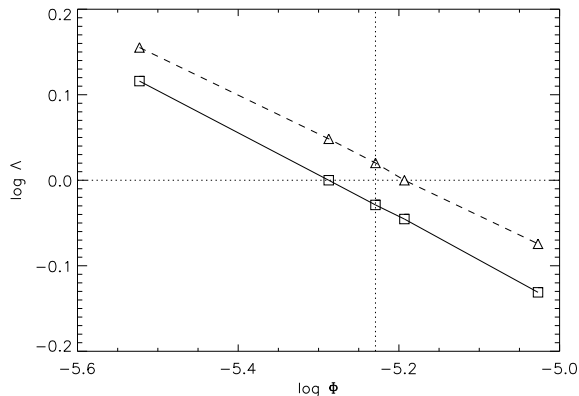


Figure 1. Λ as a function of Φ for ζ Puppis: the boxes (connected by solid line) show computations with line branching and the triangles (connected with dashed line) show computations with resonance line scattering only. The dotted horizontal line is $\Lambda = 1.0$ (self-consistent model) and the vertical dotted line indicated the observed mass-loss rate (from Puls et al. 1996). The Λ values are accurate to around ± 0.01 dex.

The calculations yield a self-consistent ($\Lambda = 1$) mass-loss rate for ζ Puppis of $5.16 \times 10^{-6} M_{\odot} \text{ yr}^{-1}$ if line branching is included and $6.41 \times 10^{-6} M_{\odot} \text{ yr}^{-1}$ if only resonance scattering is permitted. A sufficient number of packets were used that these values of Φ are correct to better than ± 2 per cent. Thus the differential effect of line branching in the ζ Puppis model is a reduction in the mass-loss rate by around 20 per cent.

This reduction occurs as a result of photon leakage: the net effect of line branching is the transfer of packets from frequency ranges with many strong lines to regions with fewer lines. This reduces the average number of lines with which a packet interacts and thus reduces the mass-loss rate. This effect is illustrated by Fig. 2 which shows the number of line scatterings that packets undergo when line branching is allowed compared to when it is not. Clearly, line branching significantly reduces the number of packets that undergo multiple (> 10) line scattering events. Of course the wind is sufficiently diffuse that, in both cases, the radiative acceleration is dominated by the large number of packets which undergo relatively few scattering and so the differential effect is relatively small (the wind performance number for the ζ Puppis model is only $\eta = 0.56$). Clearly, however, the effect will be bigger when multiply scattered packets become more dominant: i.e. when $\eta > 1$.

Fig. 3 shows the fractional contribution to the energy deposition rate from all the ions included in the ζ Puppis modelling. These were computed by summing the contributions to the energy deposition rate from line scattering for each ion during the Monte Carlo simulation, not by performing separate computations with lines of only one ion at a time. The results shown are from a calculation in which branching was included. For ζ Puppis the global mass-loss rate has significant contributions from Fe and from several of the light elements (S, Ar, N, O, C). When branching is not permitted the relative contributions of the elements are very similar except that iron contributes very slightly more: this is expected since the iron group elements have the most

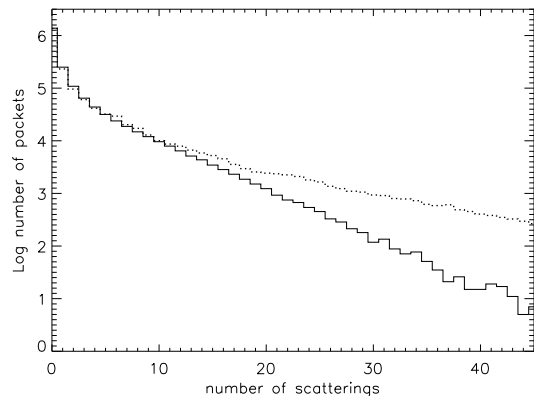


Figure 2. The number of packets versus the number of line scatterings for ζ Puppis from Monte Carlo simulations with a total of 2×10^6 packets. The solid histogram shows a simulation where line branching is allowed. The dotted histogram is the case where only resonance scattering is included.

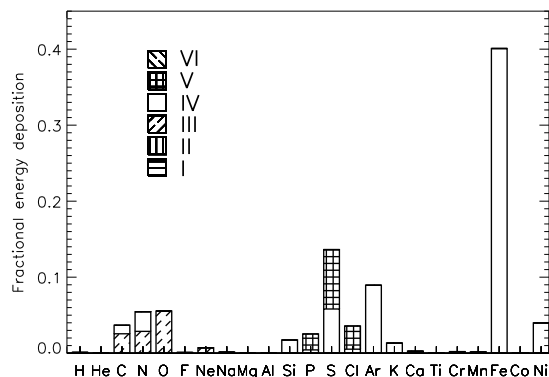


Figure 3. The relative importance of the different elements/ions to the mass-loss-rate for ζ Puppis. The chart shows the fraction of energy deposited in the wind by each element in a Monte Carlo simulation including branching. The fractions are not significantly different if branching is neglected. The bars for each element are subdivided by ionisation stage. Note that the fractions do not sum to 1.0 because of the contribution of scattering by free electrons (not shown).

complex spectra with many bunches of lines at similar wavelengths meaning that they are the most sensitive to photon leakage.

These results must be put into context regarding their relevance to our understanding of massive stars. Firstly, let us compare the derived mass-loss rates for ζ Puppis with those derived from models made by others. AL85 adopted a slightly smaller stellar mass ($40 M_{\odot}$) and higher terminal velocity (2600 km s^{-1}) than used here and obtained a mass-loss rate for ζ Puppis of $5.2 \times 10^{-6} M_{\odot} \text{ yr}^{-1}$ from their standard model, with values ranging from about $4 - 7 \times 10^{-6} M_{\odot} \text{ yr}^{-1}$ from their models with different treatments of ionisation and assumed velocity law. This is in good agreement with the mass-loss rate derived here with resonant scattering only (AL85 did not attempt to include line branching in their calculations). Using the parameters from

Table 2, the VdKL00 mass-loss recipe gives a mass-loss rate of $9.4 \times 10^{-6} M_{\odot} \text{ yr}^{-1}$, similar to the value quoted for ζ Puppis by VdKL00. This is a little higher than the mass-loss rate obtained here, but it is important to note (see Fig. 1) that Λ is a weak function of Φ and thus relatively small differences in the modelling approach (computation of Λ) lead to larger differences in the derived globally self-consistent value of Φ . If $\Phi = 9.4 \times 10^{-6} M_{\odot} \text{ yr}^{-1}$ is used in the modelling here, a Monte Carlo simulation (with resonance scattering only) leads to $\Lambda = 0.8$, indicating that the models used here reproduce the VdKL00 energy deposition rates adequately, to within 20 per cent. Given that many simplifying assumptions have been made here (e.g. the stellar radiation field is assumed to be black-body, a single value of T_* has been adopted for all ions at all radii, no bound-free or free-free processes are included, a core-halo approach is adopted in the modelling), some discrepancy with the VdKL00 results is expected.

From observations of $H\alpha$, Puls et al. (1996) have derived a mass-loss rate of $5.9 \times 10^{-6} M_{\odot} \text{ yr}^{-1}$ for ζ Puppis. This value is indicated by the vertical line in Fig. 1, and is in good agreement with the computed mass-loss rates discussed above. However, there is significant uncertainty in the observational mass-loss rate: estimates from radio fluxes give only $2.4 \times 10^{-6} M_{\odot} \text{ yr}^{-1}$ (Lamers & Leitherer 1993). Clumping in the wind may affect the accuracy of these determinations although this effect should be small for OB stars (Kudritzki & Puls 2000). In view of the large observational uncertainty in the mass-loss rate, the effect of line branching can be regarded as small and, for the present, is not important for modelling mass-loss from ζ Puppis to observable accuracy. However, the effect is not utterly negligible and upon a reduction in the observational uncertainty by a factor of a few, it should become detectable (note, however, that since stellar winds show intrinsic variability at the level of several tens per cent, time variability would also need to be taken into account in reliable modelling of mass-loss rates to such high accuracy).

5.2 Grid of models

Following on from the detailed discussion of ζ Puppis above, in this section the effects of line branching on the computed mass-loss rates are investigated for a range of OB-star models spanning roughly the same parameter space as the VdKL00 calculations. For each model (defined by the stellar parameters L_*, M_*, T_{eff} and v_{∞}), two $\Lambda(\Phi)$ curves have been computed, one with line branching included and one without. The models considered are listed in Table 3 and the $\Lambda(\Phi)$ curves are shown for each model in Fig. 4. For each model, the globally self-consistent ($\Lambda(\Phi) = 1$) mass-loss rate was found both with and without line branching included (Φ_{bran} and Φ_{res} , respectively). These are given in Table 3. The Monte Carlo errors in the mass-loss rates are less than 2 per cent. The table also gives the wind performance number (η) calculated with and without line branching, the VdKL00 mass-loss rate (Φ_{VdKL}) for comparison, the ratio of the branching to resonance-only mass-loss rates and the characteristic density of the model $\bar{\rho} = \Phi_{\text{bran}} / (4\pi R_c^2 v_{\infty})$. The models are labelled A – O, being ordered first by decreasing effective temperature and secondly by decreasing $\bar{\rho}$.

Consider first the high temperature models appropriate for O stars (A – H). For these models the $\Lambda(\Phi)$ curves (Fig. 4) are all approximately straight in log-log space around $\Lambda = 1$. The effect of line branching (i.e. the vertical offset between the two curves in Fig. 4) is relatively small for all these models – it leads to a reduction in the self-consistent mass-loss rate by between three and 25 per cent, relative to calculations which neglect branching. At a given temperature (e.g. compare models C – F) the reduction is closely correlated with the characteristic density ($\bar{\rho}$). This is expected since the effect of line branching is related to multiple scattering which is more common at high densities.

Models I – N all have $T_{\text{eff}} = 20,000$ K (early B stars). The first four of these models (I – L) have terminal velocities which are typical for stars cooler than the bi-stability jump ($v_{\infty} = 1.3v_{\text{esc}}^{\text{eff}}$ where $v_{\text{esc}}^{\text{eff}}$ is the effective escape velocity: see VdKL99,00) while the other two have higher terminal velocities, characteristic of stars hotter than the jump ($v_{\infty} = 2.6v_{\text{esc}}^{\text{eff}}$). For these models, the $\Lambda(\Phi)$ curves around $\Lambda = 1$ are more complex than for the higher temperature models discussed above (see Fig. 4): all the low temperature models have $\Lambda = 1$ close to a region in which $\Lambda(\Phi)$ passes through a plateau. These plateaus are the result of changes in the driving mechanism as a function of the density (which is determined by the value of Φ adopted in the model) and are thus physically related to the bi-stability jumps discussed by VdKL99,00. Specifically, the plateau seen here is associated with the balance between Fe III and Fe II: in models on the low-density (i.e. low- Φ) side of the plateau, Fe III is the single most important ion for driving the wind while on the high-density side Fe II provides the largest contribution. This transition in the driving mechanism leads to the complex shape of the $\Lambda(\Phi)$ curve.

These plateaus influence the effect of line branching on the derived mass-loss rates. Consider Models I and J: for these models, the vertical offset between $\Lambda(\Phi)$ computed with and without branching is comparable (see Fig. 4). For Model I, $\Lambda = 1$ occurs at values of Φ beyond the plateau, in a region where $\Lambda(\Phi)$ varies rapidly with Φ . This leads to a relatively small difference between Φ_{res} and Φ_{bran} . However, for Model J, $\Lambda = 1$ lies in the region where $\Lambda(\Phi)$ varies very slowly. This means that the difference between Φ_{res} and Φ_{bran} is much greater for this model. Models K, L and M are all similar to, but less extreme than, Model J. Conversely, Model N behaves similarly to Model I since it has $\Lambda = 1$ significantly below the plateau.

Taken together, Models I – N (and also the lower temperature Model O) indicate that the effect of line branching is generally greater at lower temperatures (B stars) than at high temperatures (O stars). They also show that subtleties in the modelling (in particular changes in the shape of $\Lambda(\Phi)$ resulting from changes in the driving mechanism around, for example, the bi-stability jumps) can influence the differential effect of line branching such that it cannot be described by a simple scaling with $\bar{\rho}$ and T_{eff} alone.

For most of the models, the mass-loss rate computed with resonance scattering agrees with that found by VdKL00 to within a factor of two or better, which is adequate given the differential nature of the calculations presented here. Those models where the agreement is slightly poorer (Models L, K, N and M) all have self-consistent mass-loss rates (Φ_{res}) which lie close to plateaus in $\Lambda(\Phi)$ – since $\Lambda(\Phi)$ varies

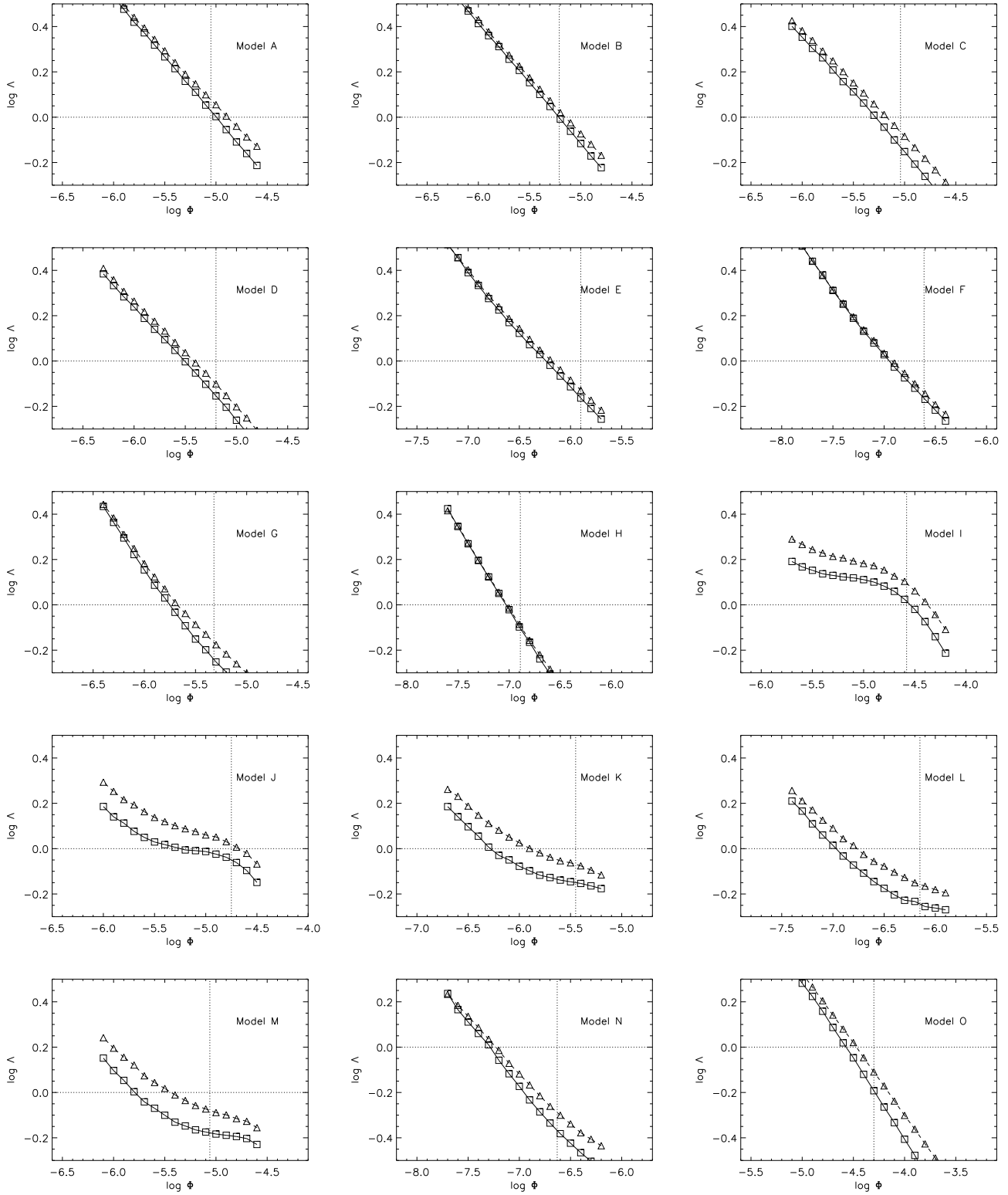


Figure 4. $\Lambda(\Phi)$ for models A to O. In each case the boxes (connected with solid lines) show the results with branching and the triangles (dashed lines) show the results without branching. The horizontal dotted line shows $\Lambda = 1.0$ (self-consistent model) and the vertical dotted line indicated the mass-loss rate from the VdKL00 recipe.

Table 3. Computed mass-loss rates for a selection of OB-star models. Φ_{res} and Φ_{bran} are the mass-loss rates computed with resonance scattering only and with line branching, respectively. Φ_{VdKL} is the mass-loss rate from the VdKL00 recipe. The terminal velocity (v_{∞}) is taken as 1.3 times the effective escape speed ($v_{\text{esc}}^{\text{eff}}$) on the cool side of the bi-stability jump and 2.6 times $v_{\text{esc}}^{\text{eff}}$ on the hot side (VdKL00). η is the wind performance number, $\eta \equiv \Phi v_{\infty} c / L_*$. $\bar{\rho} = \Phi_{\text{bran}} / (4\pi R_c^2 v_{\infty})$ is the characteristic mass density in the model. The results are accurate to $\sim \pm 2$ per cent.

Model	$\log L_*$ (L_{\odot})	M_* (M_{\odot})	T_{eff} (K)	$v_{\infty}(v_{\infty}/v_{\text{esc}}^{\text{eff}})$ (km s $^{-1}$)	$\log \Phi_{\text{bran}}$ (M_{\odot} yr $^{-1}$)	η_{bran}	$\log \Phi_{\text{res}}$ (M_{\odot} yr $^{-1}$)	η_{res}	$\log \Phi_{\text{VdKL}}$ (M_{\odot} yr $^{-1}$)	$\Phi_{\text{bran}}/\Phi_{\text{res}}$	$\log \bar{\rho}$ (g cm $^{-3}$)
A	6.0	60	50,000	2606 (2.6)	-5.01	1.24	-4.89	1.64	-5.05	0.75	-12.67
B	6.0	80	50,000	3265 (2.6)	-5.23	0.94	-5.14	1.12	-5.21	0.82	-12.99
C	6.0	60	40,000	2085 (2.6)	-5.29	0.52	-5.17	0.68	-5.04	0.76	-13.24
D	6.0	80	40,000	2612 (2.6)	-5.51	0.39	-5.42	0.49	-5.20	0.81	-13.56
E	5.5	40	40,000	2660 (2.6)	-6.24	0.23	-6.19	0.26	-5.90	0.89	-13.79
F	5.0	20	40,000	2619 (2.6)	-6.95	0.14	-6.93	0.15	-6.61	0.94	-14.00
G	6.0	60	30,000	1564 (2.6)	-5.75	0.13	-5.67	0.16	-5.32	0.83	-14.07
H	5.0	20	30,000	1964 (2.6)	-7.03	0.09	-7.02	0.09	-6.89	0.97	-14.45
I	6.0	60	20,000	521 (1.3)	-4.54	0.72	-4.37	1.07	-4.58	0.68	-13.09
J	6.0	80	20,000	653 (1.3)	-5.19	0.20	-4.67	0.68	-4.75	0.30	-13.84
K	5.5	40	20,000	665 (1.3)	-6.27	0.06	-5.90	0.13	-5.45	0.43	-14.43
L	5.0	20	20,000	655 (1.3)	-6.98	0.03	-6.77	0.05	-6.15	0.62	-14.62
M	6.0	60	20,000	1042 (2.6)	-5.78	0.08	-5.44	0.18	-5.06	0.46	-14.63
N	5.0	20	20,000	1309 (2.6)	-7.30	0.03	-7.23	0.04	-6.63	0.85	-15.25
O	6.0	60	15,000	391 (1.3)	-4.57	0.51	-4.47	0.64	-4.30 ^a	0.80	-13.49

^a This value was read from Fig 2. of VdKL00 since the mass-loss recipe (section 5 of VdKL00) does not fit this model well.

slowly in these regions relatively minor inadequacies in the models (i.e. the computation of Λ) lead to larger errors in the self-consistent value of Φ . In any case, these errors are of little concern since it can be seen from Fig. 4 that the differential effect of branching (the offset between the pairs of curves in the figure) is not a strong function of Φ .

In conclusion, for hot $\sim 40,000$ K stars with luminosity $\sim 10^6 L_{\odot}$ calculations which neglect branching overestimate the mass-loss rate by ~ 20 per cent while for lower luminosity stars with similar temperatures the effect is smaller. The overestimation factor can be larger for the cooler ($\sim 20,000$ K) B stars with similar luminosities (typically about 50 per cent and in extreme cases up to a factor of a few) and can be significantly affected by variations in the ionisation balance (and therefore wind driving mechanism) in the models.

6 WOLF-RAYET STAR

W-R stars have larger mass-loss rates (up to $\sim 10^{-4} M_{\odot}$ yr $^{-1}$) than OB-stars but comparable luminosities. LA93 and Gayley, Owocki & Cranmer (1995) have modelled line driving in W-R winds and shown that the high density means that multiple scattering is very important in these winds (the wind performance number is typically ~ 7 , far in excess of the single scattering limit). Thus, since the influence of line branching is linked to the predominance of multiple scattering, W-R star winds are likely to show a large differential effect if line branching is introduced to the calculation. This effect is quantified here.

The W-R wind model adopted for this study is that of LA93 ($M_* = 12.6 M_{\odot}$, $R_c = 2.5 R_{\odot}$, $L_* = 2.8 \times 10^5 L_{\odot}$, $v_c = 10$ km s $^{-1}$, $v_{\infty} = 2500$ km s $^{-1}$, $\beta = 1$). These parameters were chosen by LA93 to represent a generic WN5 star. The model is similar to the OB-star models discussed above, the

main differences being the temperature stratification and the element abundances. These are discussed briefly below.

As discussed by LA93 and subsequently confirmed by Schulte-Ladbeck, Eenens & Davis (1995) and Herald et al. (2000), observations suggest that there is a significant outward variation of ionisation in W-R winds. Ionisation stratification has also been predicted theoretically from W-R type models (e.g. de Koter et al. 1997). To account for this, LA93 imposed a simple variation of radiation temperature with velocity (their equation 11) which is also used here. Their standard value for the radiation temperature at v_{∞} of $\log T_R = 4.35$ is adopted here. The outward variation of electron temperature is less critical to the calculation: it is obtained from the modified Milne-Eddington temperature distribution (Lucy 1976), following LA93. In addition, the usual dilution factor (W) is replaced by the modified dilution factor (W_i) defined by LA93.

The same elemental composition used by LA93 is adopted. Thus $X = 0.0$, $Y = 0.98$ and $Z = 0.02$. The carbon, nitrogen and oxygen are taken from a WNE model (Maeder & Meynet 1987) and the other metal abundances are scaled from solar values to give $Z = 0.02$.

As in the OB-star models, the radiation field at the base of the model $r = R_c$ is assumed to be black-body with a high energy cut-off at the He II ionisation edge. This cut-off is inconsistent with the adopted ionisation structure (i.e. if there is really no radiation shortward of the He II edge then there are no photons to produce the high ionisation stages by photoionisation). However, this is of little consequence here since in reality there will be a locally produced radiation field that can produce the high ions. In addition, the calculations presented here are relatively insensitive to the wavelength cut-off in the incident radiation field since most of the input energy is at longer wavelengths: this has been checked explicitly with Monte Carlo simulations in which the high energy cut-off was placed at higher energy (by a factor

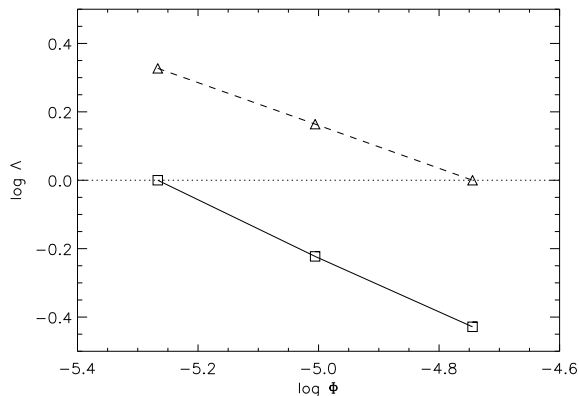


Figure 5. Λ as a function of Φ for the W-R model: the boxes (connected by solid line) show computations with line branching and the triangles (connected with dashed line) show computations with resonance line scattering only. The dotted horizontal line is $\Lambda = 1.0$ (self-consistent model). The Λ values are accurate to around ± 0.01 dex.

of ten) – the results of those simulations are not significantly different from those presented below.

The black-body temperature adopted for the incoming radiation field is $T_{\text{eff},c}$, the effective temperature determined from L_* at R_c . To allow for the higher temperatures deep in W-R winds, the line list used for the OB stars (see Section 4) was expanded to include lines from higher ionisation stages (VII and VIII) of the most important iron group elements (iron and nickel). In the calculations that follow, however, these ion stages provide a negligible contribution ($< \sim 1$ per cent) to the radiative driving because of the assumed shape of the input stellar radiation field – most of the energy is at wavelengths that are too long for the packets to interact with the strong lines of these ions.

Fig. 5 shows Λ versus Φ for W-R models computed with and without line branching in the Monte Carlo simulation. As expected, Fig. 5 shows that line branching has a far larger effect on the mass-loss calculation for a W-R star than for OB stars: the difference between Λ computed with and without branching for a given value of Φ is much greater than for any of the models discussed in Section 5. The self-consistent W-R mass-loss rate determined without branching is $1.8 \times 10^{-5} M_{\odot} \text{ yr}^{-1}$ (which is close to the value of $2.1 \times 10^{-5} M_{\odot} \text{ yr}^{-1}$ found by LA93). When line branching is included the mass-loss rate is only $5.4 \times 10^{-6} M_{\odot} \text{ yr}^{-1}$, a reduction by more than a factor of 3. Note that while some of the cool OB models discussed in Section 5 also predicted large reduction factors ($\Phi_{\text{res}}/\Phi_{\text{bran}}$), these were not because branching had such a large effect on the computed values of Λ for a given value of Φ but were because of the relative insensitivity of Λ to the value of Φ adopted in the modelling.

The magnitude of this effect can be explained following the discussion of the O stars above. Fig. 6 shows the distribution of the number of line scatterings for the W-R model. The reduction in the number of packets that are scattered many times as a result of line branching is dramatic in the W-R model: without branching, individual packets undergo up to ~ 700 line scatterings (in a simulation with 10^6 packets) but with branching included no packets undergo more

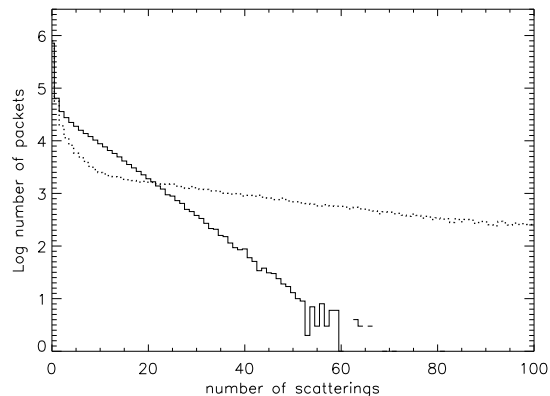


Figure 6. The number of packets versus the number of line scatterings for the W-R model from Monte Carlo simulations with a total of 10^6 packets. The solid histogram shows a simulation where line branching is allowed. The dotted histogram shows the case where only resonance scattering is permitted.

than 90 line scattering events. Comparing Figs. 2 and 6, shows that multiple scattering is much more important in the W-R model than in the ζ Puppis model. Thus photon leakage from one part of the spectrum to another has a much greater influence on the derived mass-loss rate.

Fig. 7 shows the contribution of the different ions to the mass-loss rate for the W-R model. The lower panel is from a simulation with resonant scattering only and the upper shows calculations with line branching. The W-R mass-loss rate is dominated by the iron group elements (Fe and Ni). When branching is included the relative contribution of the iron group elements drops and the lighter elements become more important: as discussed in Section 5.1, this is expected because of the greater complexity of the iron group ions. The effect here is more dramatic than in ζ Puppis, but is still small (the fractional contribution of Fe and Ni to the line driving is smaller when branching is allowed by only ~ 10 per cent).

There is some observational evidence to suggest that the wind acceleration is more gradual in W-R stars than OB stars: e.g. based on infrared data Ignace, Quigley & Cassinelli (2003) have recently suggested β values of 2–3 for a WN6 star, and they do not rule out larger values. Therefore, to investigate the sensitivity of the results presented here to the adopted value of β , calculations have been performed using the same W-R parameters as above except that $\beta = 3$ was used for the velocity law. In this case, the derived mass-loss rates were smaller: $7.2 \times 10^{-6} M_{\odot} \text{ yr}^{-1}$ and $4.4 \times 10^{-5} M_{\odot}$, with and without line branching, respectively. The differential effect of line branching is smaller here than for the $\beta = 1$ case, but is still significant (a factor of ~ 1.6).

7 CONCLUSIONS

In the previous sections, simple wind models for a range of hot stars have been used to investigate the effect of line branching on mass-loss rates. For O stars, where accurate mass-loss rates are important for evolutionary calculations,

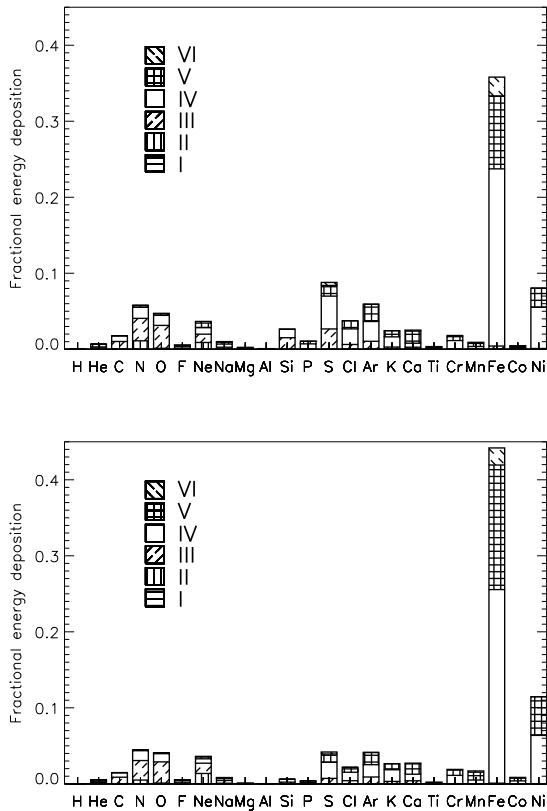


Figure 7. The relative importance of the different elements/ions to the mass-loss-rate for the W-R model. The upper panel shows the contributions when branching is included and the lower panel shows the case where only resonance scattering is included. In both cases the chart shows the fraction of energy deposited in the wind by each element. The bars for each element are subdivided by ionisation stage. Note that although the seventh and eighth stages of iron and nickel are included in the simulation they make a negligible contribution which is not shown here. The fractions do not sum to 1.0 because of the contribution of scattering by free electrons (not shown).

the overestimation is relatively small, typically < 25 per cent and is correlated with the predominance of multiple scattering. For these stars the difference in the mass-loss rate computed with and without line branching is comparable to or less than typical observational errors in O-star mass-loss rates. Thus, despite the assumption of resonant scattering, in most cases the VdKL00 mass-loss calculations are not significantly in error. In the future, however, when observational constraints become tighter it will be necessary to include line branching in realistic mass-loss calculations.

The effect of line branching in relatively cool ($\sim 20,000$ K) luminous stars (early B stars) is significantly larger than in the hotter stars (on average about 50 per cent), but it is also more sensitive to the details of the modelling.

Line branching is most important under conditions typical of a W-R star. The W-R calculations presented here suggest that neglecting line branching results in an overestimation of the mass-loss rate by a factor ~ 3 for $\beta = 1$. The effect is less severe if a larger value of β is adopted but

is still significant at least for $\beta \sim 3$. This has implications for modelling line driving in W-R stars: branching makes it significantly harder for line driving to accelerate the winds of these stars. There are many unanswered questions relating to W-R stars, particularly regarding the roles of line and continuum driving throughout their winds. But the results presented here clearly show that branching significantly influences mass-loss calculations which involve multiple scattering and that future studies of line driving in W-R stars must incorporate these effects.

ACKNOWLEDGEMENTS

I wish to thank L. Lucy for many useful discussions and insightful comments relating to this work. Thanks also to J. Vink, J. Drew, S. Owocki and, in particular, the referee A. de Koter for their comments. This work was carried out while I was a PPARC supported PDRA at Imperial College London (PPA/G/S/2000/00032).

BIBLIOGRAPHY

- Abbott D. C., Lucy L. B., 1985, *ApJ*, 288, 679 (AL85)
 Castor J. I., Abbott D. C., Klein R. I., 1975, *ApJ*, 195, 157
 Crowther P. A., Dessart L., 1998, *MNRAS*, 296, 622
 Crowther P. A., Pasquali A., De Marco O., Schmutz W., Hillier D. J., de Koter A., 1999, *A&A*, 350, 1007
 de Koter A., Heap S. R., Hubeny I., 1997, *ApJ*, 477, 792
 Gayley K. G., Owocki S. P., Cranmer S. R., 1995, *ApJ*, 442, 196
 Herald J. E., Schulte-Ladbeck R. E., Eenens P. R. J., Morris P., 2000, *ApJS*, 126, 469
 Ignace R., Quigley M. F., Cassinelli J. P., 2003, *ApJ*, in press
 Klein R. I., Castor J. I., 1978, *ApJ*, 220, 902
 Kudritzki R.-P., Puls J., 2000, *ARA&A*, 38, 613
 Kurucz R. L., Bell B. 1995, *Atomic Line Data CD-ROM No. 23*, Cambridge, Mass.: S.A.O.
 Lamers H. J. G. L. M., Leitherer C., 1993, *ApJ*, 412, 771
 Lamers H. J. G. L. M., Nugis T., 2002, *A&A*, 395, L1
 Leitherer C. et al., 1996, *PASP*, 108, 996
 Lucy L. B., 1976, *ApJ*, 205, 482
 Lucy L. B., Solomon P. M., 1970, *ApJ*, 159, 879
 Lucy L. B., Abbott D. C., 1993, *ApJ*, 405, 748 (LA93)
 Lucy L. B., 1999a, *A&A*, 344, 282
 Lucy L. B., 1999b, *A&A*, 345, 211
 Lucy L. B., 2002, *A&A*, 384, 725
 Lucy L. B., 2003, *A&A*, 403, 261
 Maeder A., Meynet G., 1987, *A&A*, 182, 243
 Morton D. C., 1967, *ApJ*, 147, 1017
 Nugis T., Lamers H. J. G. L., 2002, *A&A*, 389, 162
 Onifer A. J., Gayley K. G., 2003, *ApJ*, 590, 473
 Owocki S. P., Gayley K. G., 1999, in *IAU Symp. 193: 'Wolf-Rayet Phenomena in Massive Stars and Starburst Galaxies'*, p. 157
 Puls J. et al., 1996, *A&A*, 305, 171
 Schaerer D., de Koter A., 1997, *A&A*, 322, 598
 Schulte-Ladbeck R. E., Eenens P. R. J., Davis K., 1995, *ApJ*, 454, 917
 Springmann U., Puls J., 1998, *ASP conf. Ser. 131*, 286

- Vink J. S., de Koter A., Lamers H. J. G. L. M., 1999, A&A, 350, 181 (VdKL99)
- Vink J. S., de Koter A., Lamers H. J. G. L. M., 2000, A&A, 362, 295 (VdKL00)
- Vink J. S., de Koter A., Lamers H. J. G. L. M., 2001, A&A, 369, 574
- Vink J. S., de Koter A., 2002, A&A, 393, 543